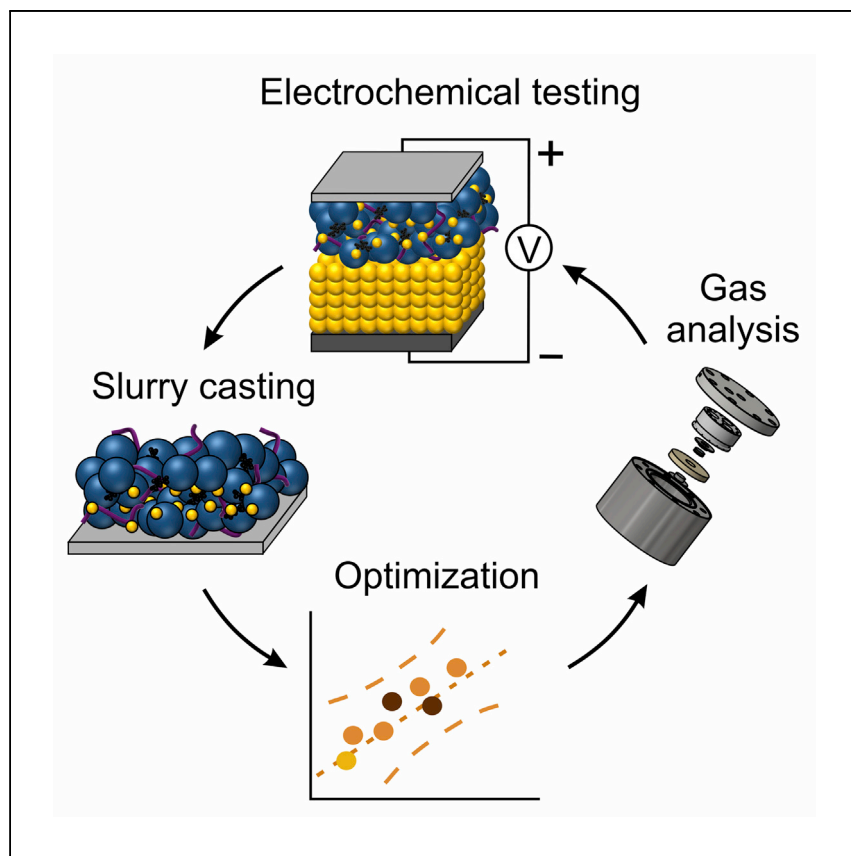


Article

Design-of-experiments-guided optimization of slurry-cast cathodes for solid-state batteries



Teo et al. apply a statistical approach, DoE, to facilitate the transition from pelletized to slurry-cast cathodes for solid-state batteries. Datasets from electrochemical and mechanical tests are used to build a model that allows effective tailoring of the slurry recipe. The DoE predictions/results are evaluated using various analytical techniques.

Jun Hao Teo, Florian Strauss, Đorđije Tripković, ..., Matteo Bianchini, Jürgen Janek, Torsten Brezesinski

jun.teo@kit.edu (J.H.T.)
juergen.janek@kit.edu (J.J.)
torsten.brezesinski@kit.edu (T.B.)

Highlights

Statistical optimization of slurry-cast NCM cathodes for solid-state batteries

Cycling performance and processability correlate with binder chemistry and content

Design of experiments (DoE) results are corroborated experimentally

Operando gas analysis reveals (electro-)chemical binder instability

Article

Design-of-experiments-guided optimization of slurry-cast cathodes for solid-state batteries

Jun Hao Teo,^{1,6,*} Florian Strauss,¹ Đorđije Tripković,² Simon Schweidler,¹ Yuan Ma,¹ Matteo Bianchini,^{1,2} Jürgen Janek,^{1,3,4,*} and Torsten Brezesinski^{1,5,*}

SUMMARY

Laboratory research into bulk-type solid-state batteries (SSBs) has been focused predominantly on powder-based, pelletized cells and has been sufficient to evaluate fundamental limitations and tailor the constituents to some degree. However, to improve experimental reliability and for commercial implementation of this technology, competitive slurry-cast electrodes are required. Here, we report on the application of an approach guided by design of experiments (DoE) to evaluate the influence of the type/content of polymer binder and conductive carbon additive on the cyclability and processability of $\text{Li}_{1+x}(\text{Ni}_{0.6}\text{Co}_{0.2}\text{Mn}_{0.2})_{1-x}\text{O}_2$ (NCM622) cathodes in SSB cells using lithium thiophosphate solid electrolytes. The predictions are verified by charge-discharge and impedance spectroscopy measurements. Furthermore, structural changes and gas evolution are monitored via X-ray diffraction and differential electrochemical mass spectrometry, respectively, in an attempt to rationalize and support the DoE results. In summary, the optimized combination of polymer binder and conductive carbon additive leads to high electrochemical performance and good processability.

INTRODUCTION

Advances in electrochemical energy storage have been going at breakneck pace in recent years. This is largely attributed to progress in mobile devices. Conventional Li-ion batteries (LIBs) have played a major role in improving connectivity in a globalized world. As battery technologies progressed, novel concepts of integrating them into existing systems have emerged, ranging from solving environmental problems to revolutionizing the century-old automobile industry. State-of-the-art LIBs remain the first choice for energy-storage systems. However, LIBs have limitations. First, they do not yet possess the desired energy and power densities for mobility and transportation applications. Second, they possess an inherent safety concern because of the flammable components in the system, which have led to well-documented spontaneous combustion and explosions.¹

Solid-state batteries (SSBs) are widely seen as the next generation of lithium batteries that could potentially overcome the previously mentioned limitations.² SSBs may possess increased power and energy densities, improved safety conditions, and a larger operating temperature window. These advantages would allow them to be used in a wider range of applications. The main components of SSBs are the cathode composite, the solid-electrolyte separator layer, and the anode composite (or Li metal). The cathode composite is a solid dispersion of solid electrolyte, active material, and additives. The separator layer is a densely packed solid electrolyte with sufficient mechanical stability and high tolerance against dendrite growth, in the

¹Battery and Electrochemistry Laboratory, Institute of Nanotechnology, Karlsruhe Institute of Technology (KIT), Hermann-von-Helmholtz-Platz 1, 76344 Eggenstein-Leopoldshafen, Germany

²BASF SE, Carl-Bosch-Str. 38, 67056 Ludwigshafen, Germany

³Institute of Physical Chemistry & Center for Materials Science, Justus-Liebig-University Giessen, Heinrich-Buff-Ring 17, 35392 Giessen, Germany

⁴Twitter: @Janek_Lab_JLU

⁵Twitter: @TBrezesinski

⁶Lead contact

*Correspondence: jun.teo@kit.edu (J.H.T.), juergen.janek@kit.edu (J.J.), torsten.brezesinski@kit.edu (T.B.)

<https://doi.org/10.1016/j.xcrp.2021.100465>



case of a Li metal anode.³ In contrast, LIBs have a porous separator filled with flammable organic electrolyte.

There are two main groups of solid electrolytes under consideration for next-generation SSBs, namely, sulfides/oxides (glasses, ceramics, and glass-ceramics) and polymers. Each has advantages and disadvantages. The sulfide (thiophosphate) solid electrolytes have high room-temperature ionic conductivities² and low elasticity moduli and shear strengths,^{4,5} and they possess good processability at low temperatures. However, they are highly reactive under ambient conditions, requiring them to be processed in a dry environment. In addition, the reaction with water (atmospheric conditions) generates toxic gases such as H₂S, thus contributing to a potentially new safety issue. Moreover, sulfide solid electrolytes have narrow electrochemical stability windows and show significant interfacial reactivity at both low and high voltages.⁶ In contrast, the oxide ceramic electrolytes are relatively more stable under ambient conditions and do not generate toxic gases when exposed to humidity. Their electrochemical stability windows are also larger compared with those of sulfides. However, they possess lower room-temperature ionic conductivities, are brittle, and typically synthesized at high temperatures. Furthermore, processing of oxide solid-electrolyte SSBs is extremely challenging. Oxides are true ceramic materials with high elasticity moduli and shear strengths, making the formation of low-impedance interfaces between the solid electrolyte and the cathode active material (CAM) achievable only at high temperatures.⁷ Lastly, the polymers are often considered ideal solid electrolytes, possessing strong dendrite growth resistance and improved safety and reliability, but they still show too low conductivity.^{8,9}

In the last few years, there has been an exponential growth in the research and development of predominantly powder-based, pelletized SSBs, ranging from the tailored composition of the cathode composite,^{10,11} particle size,¹² cell-fabrication pressure,¹³ and stack pressure applied during electrochemical cycling^{14–17} to the operation temperature.¹⁸ Such cells often show good electrochemical performance. However, those that are typically used on a laboratory level are not scalable. Furthermore, variances between assembled SSBs are commonly observed for pelletized cells, resulting in discrepancies of experimental results. To be cost competitive with LIBs and exhibit improved reliability, SSBs have to transition toward sheet-based designs.

The concept of sheet-based (sulfide) SSBs has been thoroughly discussed and is regarded as feasible.^{19,20} However, although there are almost three decades of experience in processing of porous electrode sheets for LIB applications, there is little experience in processing of compact solid-state electrode sheets. And there are still numerous challenges for the production of sheet-based SSBs, the first of which is the formulation of a slurry recipe (choice of solvent, cathode components, etc.). For example, the application of sulfide solid electrolytes requires solvents to be nonpolar to avoid unwanted side reactions. Consequently, the polymer binders have to be nonreactive, are preferably soluble in nonpolar solvents, and should provide sufficient mechanical stability to the fabricated electrode sheets and not severely affect the ionic conductivity of the solid electrolyte.²¹ Furthermore, binders have different functional groups, and it is crucial to understand their interaction with the different components in the cathode composite and how that influences the SSB operation.

The combinations of solvent and binder alone highlight the considerable number of parameters (viscosity, adhesion force, etc.) contributing to the electrode quality and

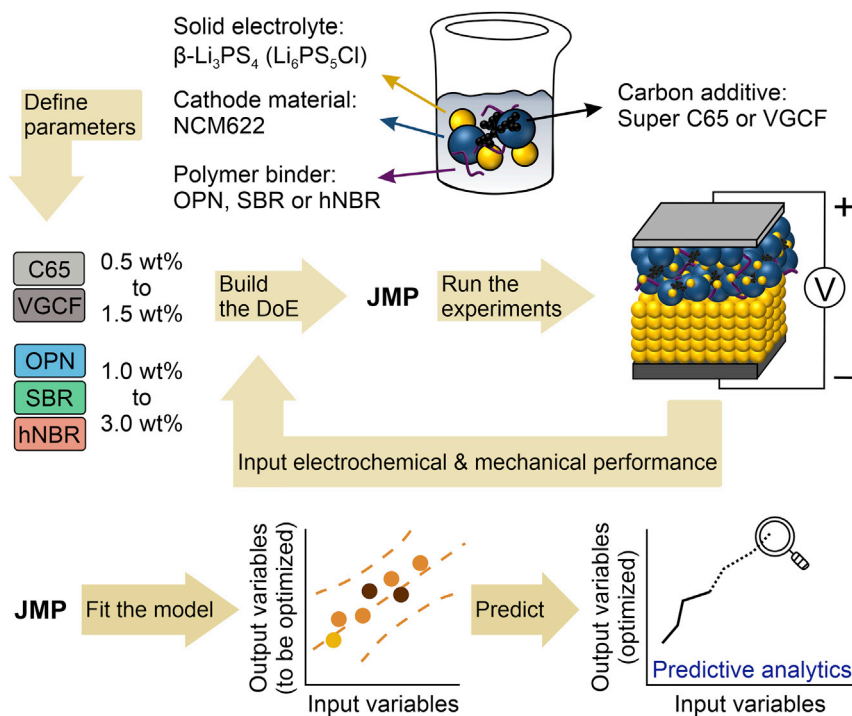
ultimately the electrochemical performance. Under normal circumstances, the number of experiments required increases on a factorial scale with the number of parameters under consideration. In addition, when dealing with a large dataset, with large numbers of possible combinations between parameters, important correlations among them may be missed. Here we use a design of experiments (DoE) approach to tailor the cathode-composite-sheet preparation process for improved electrochemical performance. DoE is a well-established method for optimizing experimental sets with the goal of maximizing statistical power and/or minimizing the number of trials. We exploit DoE to reduce the number of experiments without compromising information quality (statistical power) due to the relatively cost- and labor-intensive process of electrode-sheet preparation.

In this work, we describe the screening of different types of polymer binders and carbon additives and their respective contents with the help of a DoE approach (we have several fixed parameters for the slurry recipe, such as the choice of solvent and cathode active material). Three candidates for binders and two candidates for additives are selected, and the design is evaluated using the statistical software JMP 14 (SAS Institute Inc.). A set number of electrode sheets are created with various combinations of the binder type/content and carbon type/content, which are subjected to electrochemical and mechanical tests in SSB full cells with a carbon-coated $\text{Li}_4\text{Ti}_5\text{O}_{12}$ (LTO) anode. We then feed this data back into the software to build a simple linear model that allows the prediction and optimization of the materials' combination. Finally, we use a combination of *ex situ* and *operando* techniques to better understand the cell cyclability and justify the predictions.

RESULTS AND DISCUSSION

DoE approach

The goal of the present DoE-guided approach was the optimization of slurry-cast cathodes for application in SSBs with regard to the type and content of polymer binder and carbon additive (Scheme 1). The first step involved defining the experimental conditions. As mentioned, we focused mainly on the variation of the material-related parameters and therefore fixed the process-related ones. The material-related parameters were defined as follows: (1) carbon type (Super C65 carbon black or vapor-grown carbon fibers [VGCF]) in categorical roles, (2) carbon content (0.5–1.5 wt %) in continuous roles, (3) binder type (polyisobutene [OPN], poly(styrene-co-butadiene) rubber [SBR], or hydrogenated nitrile butadiene rubber [hNBR]) in categorical roles, and (4) binder content (1.0–3.0 wt %) in continuous roles, with “categorical” implying that the variables are represented as they are and “continuous” implying that the variables can be set to any value between the lower and the upper limits. These made up the first input variables needed for the program to design a set of experiments. The required number of runs in this study was 23 (Table S1). Then, all experiments were carried out, and the results were evaluated in terms of capacity retention and specific discharge capacity after 20 cycles and mechanical properties (bendability and punchability of the cathode sheet). These formed the second set of input variables. After preparing all 23 electrodes (details in the Supplemental Experimental Procedures) and performing the necessary tests, the results were analyzed in JMP 14. To probe the possible interactions among variables, we used the response surface model (RSM) to fit the data. While evaluating the model, it is crucial to avoid overfitting. Overfitted models are unnecessarily complex. They fit better to the dataset but produce poorer predictions. A way to avoid overfitting is to remove variables of small significance, resulting in a more robust model while maintaining a high adjusted R^2 value. The *p* value represents the probability of an outcome under the assumption that the null hypothesis is true. In this study, the



Scheme 1. Schematic overview of the DoE-guided approach for tailoring of slurry-cast cathodes in SSBs

null hypothesis was defined as “The input variables (with/without their interactions) do not influence the electrochemical performance and processability of the cathode sheet.” A high p value for an input variable would mean that it does not strongly affect the electrochemical performance and processability of the cathode sheet. Hence, variables with $p > 0.05$ were removed from consideration when building the model. An advantage of using the adjusted R^2 value over the R^2 value is that it takes interactions among variables into account and is a better representation of a model that has multiple variables. The closer the adjusted R^2 value is to 100%, the better the model is at predicting the output variables.

For high prediction power, the number of parameters was reduced to eight and six for the capacity retention and specific discharge capacity, respectively. When considering both electrochemistry and mechanical outputs, the minimum number of parameters required was six (Table S2).

Optimizing for electrochemical performance

Monitoring capacity retention helps to quantify the cell degradation, whereas the specific discharge capacity is an indication of the practical energy storage capability of the cell. In general, the large scattering of the electrochemical performance among cells of different binder/carbon combinations already indicates the strong dependence on the material type and content (Figure S1). To gain more insight on how each parameter affects the electrochemical performance, the selected parameters from all 23 cells were fed into the statistical program to create prediction profiles independent from one another.

The plots in Figure 1 show the corresponding combinations of material parameters and their influence on the specific discharge capacity and capacity retention. The

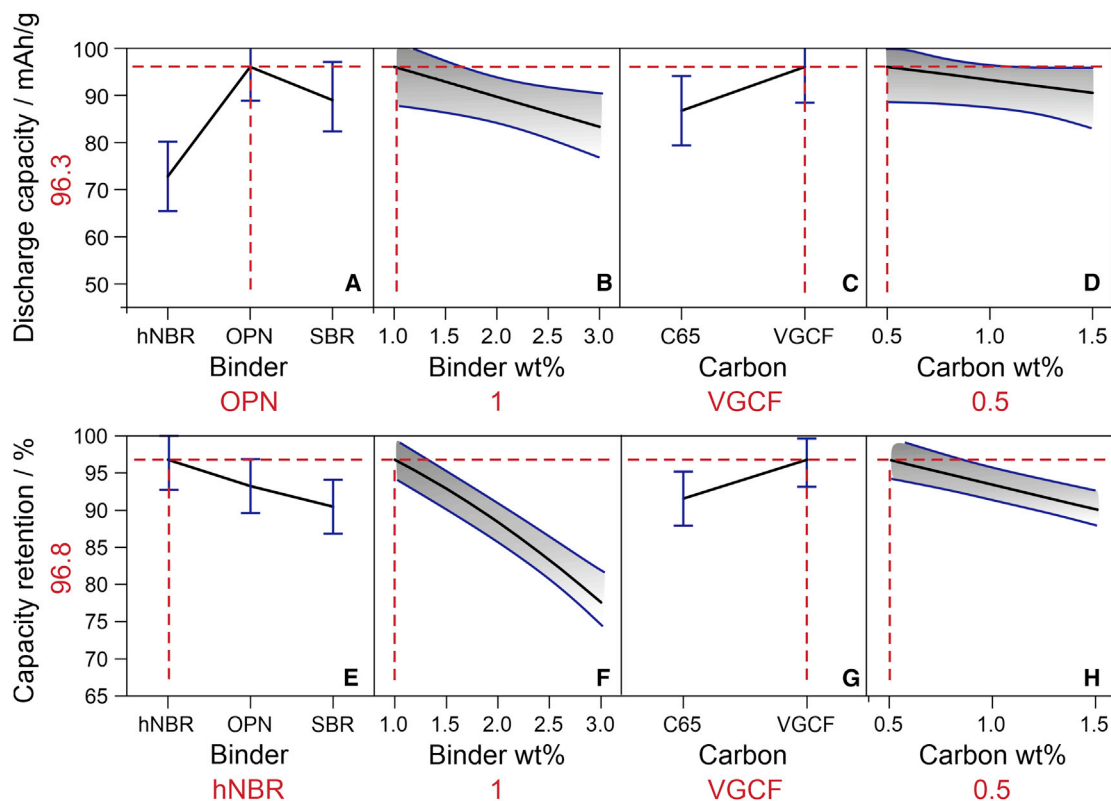


Figure 1. Prediction profiles generated for the optimization of electrochemical performance

The optimum combinations for (A–D) 20th-cycle specific discharge capacity and (E–H) capacity retention after 20 cycles are extrapolated to be OPN (1.0 wt %)/VGCF (0.5 wt %) and hNBR (1.0 wt %)/VGCF (0.5 wt %), respectively.

steeper the slope of the line, the larger the influence of the parameter. The intersection with the dashed red lines represents the optimal value for the respective variable. The blue lines for the binder and carbon type represent the 95% confidence interval for each categorical value. For the binder and carbon content, the gray areas encompassed by the blue curves represent the 95% confidence band on a continuous level. Looking at the generated profiles, the magnitude of influence of the input variables on both the specific discharge capacity and the capacity retention decreases from binder type to binder content, to carbon type, and lastly to carbon content. The optimal recipe shown in Figures 1A–1D to maximize the specific discharge capacity predicted achieving ~96 mAh/g_{NCM622} after 20 cycles. This recipe would require OPN as the polymer binder and VGCF as the conductive additive, with contents of 1.0 and 0.5 wt %, respectively. In comparison, when optimizing for capacity retention (Figures 1E–1H), a recipe resulting in ~97% would require a combination of 1.0 wt % hNBR and 0.5 wt % VGCF.

In summary, the only difference in the independent optimization of these two electrochemical parameters was the binder material (Figures 1A and 1E). For optimized capacity retention, apparently hNBR yielded the best result. However, the main reason for this is that the initial specific discharge capacity was the lowest among the three binder types (~30 mAh/g_{NCM622} lower than for OPN). In both cases, the optimal value for binder was 1.0 wt % (Figures 1B and 1F). The need for low binder content can be attributed to the employed polymers being insulating in nature, and high content increases the resistance by impeding charge transfer.^{22,23} However, in comparing the slope for binder content, a larger influence on capacity retention than

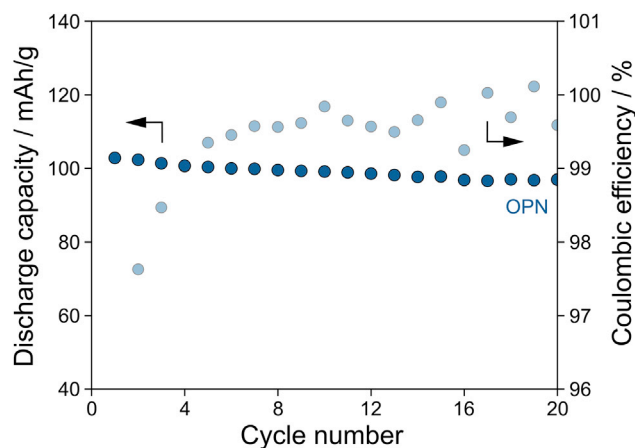


Figure 2. Cycling performance of electrochemically optimized cathodes

Specific discharge capacity (dark blue) over 20 cycles and corresponding Coulombic efficiency (light blue) of a slurry-cast cathode (uncoated NCM622, β - Li_3PS_4) with OPN binder (1.0 wt %) and VGCF conductive additive (0.5 wt %). LTO and β - Li_3PS_4 served as the pellet anode and solid-electrolyte separator, respectively, in the SSB cell. The electrochemical data represent the optimal recipe for maximum capacity and correspond to DoE run 1 (see Table S1).

on specific discharge capacity is apparent. The profiles (along the x axis) are interdependent, and the steeper slope could result from its dependence on hNBR as the choice of binder. As for carbon-related parameters, VGCF was chosen as the optimal choice in both cases (Figures 1C and 1G). This can be explained, at least partly, by its lower specific surface area compared with Super C65 (by a factor of ~ 6). It has been reported recently that the presence of carbon additives may potentially activate and accelerate the formation of decomposition products,^{24–26} which leads to impedance buildup. A lower specific surface area may reduce the number of contact points between the electronically conductive carbon and the thiophosphate solid-electrolyte particles, thereby reducing the probability of side reactions.^{27,28} Lastly, carbon content of 0.5 wt % was found to be optimal in both cases (Figures 1D and 1H). The more gradual slope compared with the other parameters reveals that it has a minor influence on the overall electrochemical performance of the cell.

In the present work, the specific discharge capacity was chosen to represent the electrochemical performance, because the capacity retention was not an accurate starting indicator. This is because a low-capacity cell would show inherently higher capacity retention. However, capacity retention could work as a second indicator for cells delivering similar discharge capacities. Hence, in this study, the SSB cell optimized for electrochemical performance is based on the specific discharge capacity and is represented by a slurry-cast cathode with 1.0 wt % OPN and 0.5 wt % VGCF. This recipe has been investigated in one of the 23 experimental runs (DoE run 1, see Table S1). The cyclability at a rate of C/10 and 25°C of the cell using uncoated $\text{Li}_{1+x}(\text{Ni}_{0.6}\text{Co}_{0.2}\text{Mn}_{0.2})_{1-x}\text{O}_2$ (NCM622) CAM ($\sim 12 \text{ mg}_{\text{NCM622}}/\text{cm}^2$ areal loading) is shown in Figure 2, in which the initial specific charge and discharge capacities amounted to ~ 157 and $103 \text{ mAh/g}_{\text{NCM622}}$, respectively, corresponding to $\sim 66\%$ Coulombic efficiency. The Coulombic efficiency stabilized above 99% after four cycles. After 20 cycles, the capacity decayed to $\sim 96 \text{ mAh/g}_{\text{NCM622}}$. This correlates with a fade rate per cycle of $\sim 0.36\%$.

Optimizing for electrochemical performance and processability

Optimization for electrochemical performance established that low binder content is necessary for optimum cyclability. However, slurry-cast cathodes with low binder

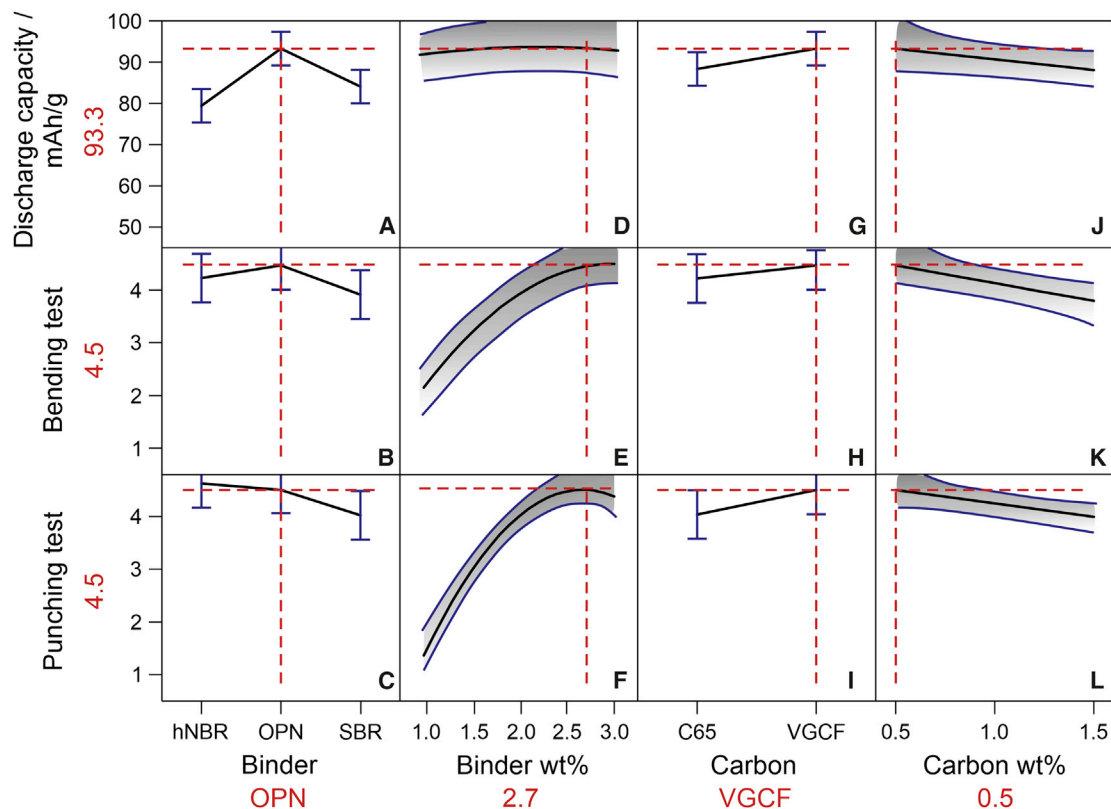


Figure 3. Prediction profiles generated for the optimization of electrochemical performance and processability

The optimum combination for the (A, D, G, and J) 20th-cycle specific discharge capacity, (B, E, H, and K) bending test, and (C, F, I, and L) punching test is OPN (2.7 wt %)/VGCF (0.5 wt %). The scale used for the bending and punching tests is detailed in the [Experimental Procedures](#) and [Figure S2](#).

content are usually prone to delamination and cracking during cell preparation. For practical applications, the electrodes have to be mechanically stable to fulfill the requirements for roll-to-roll processing. The mechanical stability was probed via two in-house mechanical tests ([Figure S2](#)), which simulated common stages in an industrial fabrication process.¹⁹ The scaling values from 1 to 4 were defined as being continuous and should be considered goodness values (they do not represent the theoretical upper and lower limits). In fact, JMP 14 extrapolated a system with processability above our set limit, which meant a slurry-cast cathode with mechanical properties better than what was observed during testing. For electrochemical performance, the 20th-cycle specific discharge capacity was chosen as the only input variable for the reasons explained earlier. Bending and punching tests were used as input variables to represent the processability of the electrode sheets. The generated profiles in [Figure 3](#) show that there are certain trade-offs to be expected among the material-related variables. OPN binder was found to be the preferred choice for achieving slurry-cast cathodes with both good electrochemical performance and good processability. The profiles indicate that the choice of binder is the bottleneck for electrochemical performance ([Figure 3A](#)) but only plays a minor role in processability ([Figures 3B](#) and [3C](#)). However, the profiles for binder content display a small influence on electrochemical performance ([Figure 3D](#)), whereas the content is a significant bottleneck for processability ([Figures 3E](#) and [3F](#)). Both bending and punching tests indicated that higher binder content is necessary for optimum processability. A larger fraction of polymer binder leads to a more compliant and processable system. However, in exchange for improved processability, the electrochemical performance would be negatively affected. To optimize for both

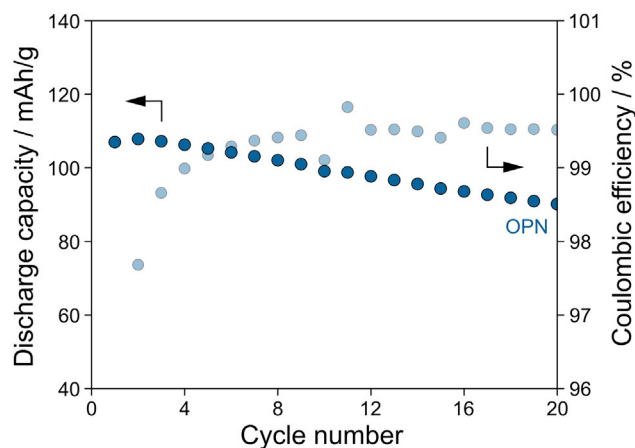


Figure 4. Cycling performance of electrochemically and processability optimized cathodes
Specific discharge capacity (dark blue) over 20 cycles and corresponding Coulombic efficiency (light blue) of a slurry-cast cathode (uncoated NCM622, β - Li_3PS_4) with OPN binder (2.7 wt %) and VGCF conductive additive (0.5 wt %). LTO and β - Li_3PS_4 served as the pellet anode and solid-electrolyte separator, respectively, in the SSB cell. The electrochemical data represent the extrapolated optimum combination for maximum electrochemical performance and processability.

electrochemical performance and processability, a recipe with 2.7 wt % binder content would be required. This trade-off between electrochemical performance and mechanical stability is also in agreement with modeling studies performed on composite cathodes in SSBs.²⁹ As for carbon-related parameters (Figures 3G–3L), the slope in the prediction profiles is generally flatter than that of the binder-related parameters, suggesting a smaller degree of influence on both the electrochemical performance and the processability of the cathode sheets. Nevertheless, VGCF with content of 0.5 wt % was chosen as the optimized fraction of conductive additive.

In summary, the optimized recipe regarding electrochemical performance and cathode processability was equally composed of 2.7 wt % OPN and 0.5 wt % VGCF. This is somewhat different from the recipe that was solely optimized with regard to electrochemical performance, in which only 1.0 wt % OPN was included. The VGCF content was similar for both recipes.

Representative cycling data at a rate of C/10 and 25°C of the SSB cell using uncoated NCM622 CAM (optimized for both electrochemistry and processability) are shown in Figure 4. The initial specific charge and discharge capacities were ~147 and 107 mAh/g_{NCM622}, respectively, corresponding to ~73% Coulombic efficiency. We hypothesize that the higher Coulombic efficiency (by ~7%) results from more extensive coverage of the NCM622 secondary particles with polymer binder, i.e., fewer solid electrolyte/CAM contact points for performance-decreasing (electro-)chemical reactions to occur. After 20 cycles, the capacity decayed to ~90 mAh/g_{NCM622}. This corresponds to a fade rate per cycle of ~0.84%, which is about twice that of the cell optimized for electrochemical performance only. With a measured 20th-cycle specific discharge capacity of ~90 mAh/g_{NCM622}, compared with the extrapolated value of 93 mAh/g_{NCM622}, this suggests that the model built in JMP 14 from the DoE approach is quite robust. The long-term cycling performance is shown in Figure S3.

Investigating binder limitations

Applying the DoE approach led us to an optimized recipe for the fabrication of slurry-cast NCM622 cathodes. As we have shown, both binder type and content

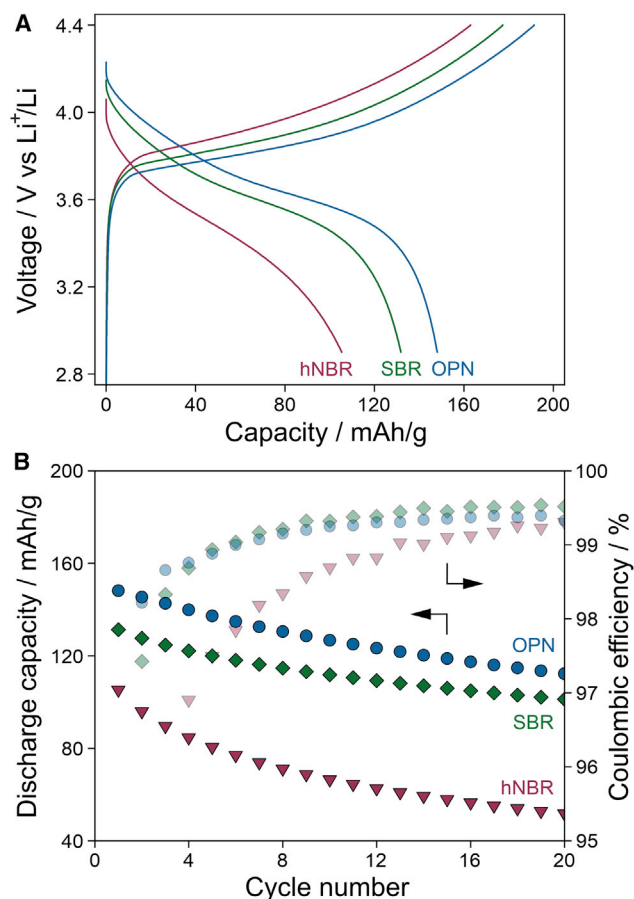


Figure 5. Cycling performance of SSB cells using different polymer binders

(A) First-cycle charge/discharge curves of slurry-cast cathodes (uncoated NCM622, β -Li₃PS₄) with 2.0 wt % polymer binder (blue, OPN; green, SBR; pink, hNBR) and 1.0 wt % VGCF conductive additive. LTO and Li₆PS₅Cl served as the pellet anode and solid-electrolyte separator, respectively, in the SSB cells.

(B) Specific discharge capacities (dark blue/green/pink) over 20 cycles and corresponding Coulombic efficiencies (light blue/green/pink).

have the strongest influence on electrochemical performance and sheet processability (carbon additives exert a minor influence in both cases). To understand the differences in cyclability and the role of the polymer binder, we subsequently probed the respective SSB cells by means of electrochemical impedance spectroscopy (EIS), electron microscopy, X-ray diffraction (XRD), and differential electrochemical mass spectrometry (DEMS), see details in the Supplemental Experimental Procedures. To this end, slurry-cast cathode|Li₆PS₅Cl|LTO cells were investigated, with the positive electrode consisting of uncoated NCM622, β -Li₃PS₄, 1.0 wt % VGCF, and 2.0 wt % OPN, SBR, or hNBR binder. This carbon/binder combination was chosen to maximize the electrochemical performance while remaining mechanically stable and reproducible on the laboratory level. Hence, instead of the recommended 2.7 wt % content, a 2.0 wt % binder sheet was used. Moreover, Li₆PS₅Cl was used in the solid-electrolyte separator layer to minimize detrimental effects from low room-temperature ionic conductivity.

Figure 5A depicts the initial charge/discharge curves at a rate of C/10 and 25°C for the different polymer binders. As is evident, the cell containing OPN was capable of

delivering the largest specific charge and discharge capacities of ~ 191 and 148 mAh/g_{NCM622}, respectively, resulting in a first-cycle Coulombic efficiency of $\sim 77\%$. For SBR, slightly lower specific capacities of ~ 177 and 132 mAh/g_{NCM622} ($\sim 75\%$ Coulombic efficiency) were achieved, and hNBR showed the lowest values of ~ 163 and 105 mAh/g_{NCM622} ($\sim 64\%$ Coulombic efficiency), respectively. Apart from the binder, all other SSB constituents were the same. Hence, one can assign differences in specific capacity and Coulombic efficiency to the effect of the polymer binder. This implies an improved electrochemical stability in the order of OPN > SBR > hNBR, because the initial Coulombic efficiency decreased in a similar manner. On subsequent cycling, all cells underwent a rather linear capacity fade, in which those comprising OPN or SBR lost 23%–24% of their initial specific discharge capacity in the course of 20 cycles. The Coulombic efficiency stabilized above 99% after six cycles (Figure 5B). In contrast, for the cell with hNBR, the specific discharge capacity was already reduced by $\sim 50\%$ after 20 cycles, and the Coulombic efficiency barely exceeded 99%.

To gain more insight into the factors leading to the differences in capacity retention, EIS measurements were conducted at 25°C on the SSB cells after 20 cycles. The Nyquist plots of the electrochemical impedance and the corresponding fits to the data are shown in Figure S4. Except for OPN, the EIS data were fitted assuming an $R_1 + (R_2/Q_2)(R_3/Q_3)$ equivalent circuit. In the former case, an additional Q_4 element was included. R_1 is the resistance of the bulk solid electrolyte, R_2 is the grain-boundary resistance of the solid electrolyte, and R_3 represents the cathode interfacial resistance.³⁰ The resistances were determined by fitting semicircles to the frequency range of the respective circuit elements and taking the values of the intersection with the x axis. As expected, the bulk solid-electrolyte (separator) resistance was similar in all cases, ranging from 43–54 Ω . The calculated values for the cathode interfacial resistance were $\sim 1,250$, 1,850, and 4,200 Ω for OPN-, SBR-, and hNBR-based cathodes (0.64 cm² electrode area), respectively, confirming the results from galvanostatic cycling. Because the tested electrodes differed solely in their polymer-binder component, the EIS data further suggest the electrochemical stability is in the order of OPN > SBR > hNBR. Regarding the solid-electrolyte grain-boundary resistance, values of ~ 250 , 550, and 1,450 Ω were calculated for OPN, SBR, and hNBR, respectively. The latter resistance has been attributed in the literature to particle fracture and/or (chemo-)mechanical-driven separation.^{25,30} Hence, we suspect that these differences may be related to the different binder material's inherent capabilities to mitigate such mechanical degradation/deformation. However, the coverage of the solid-electrolyte particle surface with polymer binder, which negatively affects the ion conduction (at the grain boundaries), must also be taken into account and may have a large impact on the resistance. For instance, the acrylonitrile groups of hNBR have been reported to exhibit ion-dipole interactions with the lithium ions of thiophosphate solid electrolytes. This interaction thus could hypothetically lead to stronger coverage, resulting in larger cathode interfacial resistance.²¹ However, SBR contains aromatic units as functional groups, exhibiting weaker intermolecular forces with the solid electrolyte. OPN, which solely contains an aliphatic hydrocarbon polymer chain without functional groups, is believed to have the least chemical/physical interactions with the solid electrolyte.

Investigating inhomogeneities

Finally, we addressed the possibility of the different polymer binders of having an effect on the distribution of the electrode constituents, thereby indirectly affecting the electrochemical performance. Specifically, combined scanning electron microscopy (SEM)/energy-dispersive X-ray spectroscopy (EDS) analysis was performed on cathode cross sections. The corresponding SEM images and elemental maps are shown in Figure S5. The cross sections revealed partial occurrence of VGCF

agglomerates. Such agglomerates were more visible in the cathodes containing SBR or hNBR. Overall, the SEM imaging and EDS mapping indicated that in terms of homogeneity, the carbon additive in particular is seemingly better distributed in the cathodes using OPN. This may help in achieving improved electronic conduction, which is especially important for sheet-based electrodes, in which insulating polymer binder reduces the ionic and electronic partial conductivities. Regarding porosity, we found no apparent difference among the three binders.

Inhomogeneity in the cathode composite may lead to the appearance of inactive CAM fractions, causing decreased capacities.^{31,32} The occurrence of inactive NCM622 can be observed from the remaining 003 reflection at the initial 2θ position (as seen for the pristine CAM). To eliminate the possibility that the differences in electrochemical performance among polymer binders are related to inactive fractions of CAM, *ex situ* XRD measurements were carried out. The XRD patterns for all three slurry-cast cathodes showed a similar 003 peak shape (in charged state), with the reflection shifted to lower 2θ values (Figure S6). This confirms the absence of inactive NCM622. However, the asymmetric shape suggested differences in the state-of-charge (SOC) homogeneity, as usually observed for SSBs.³¹ The unit-cell volume after the first charge cycle was examined by means of Rietveld-refinement analysis. This allowed comparison of the lattice parameters with those of NCM622 in a liquid-electrolyte-based cell (used as a reference), in which conclusions can be drawn about the degree of delithiation (Figure S7). NCM622 CAM (reference) was cycled in a half-cell configuration under identical conditions to the SSB cells. The initial specific charge capacities calculated from the $x(\text{Li})$ were ~ 187 , 176, and 171 mAh/g_{NCM622} for OPN, SBR, and hNBR, respectively. This is in good agreement with the measured values (~ 196 , 183, and 165 mAh/g_{NCM622}). Differences can be attributed to errors in the estimation of $x(\text{Li})$. In addition, these estimations rely on direct comparisons between solid-electrolyte cells (*ex situ*) and liquid-electrolyte cells (*operando*) with the same CAM, which could be unreliable because of the SSB disassembling process. Hence, an attempt on *operando* XRD was made. The specialized cell setup used is shown in Figure S8, and the analysis of the *operando* synchrotron data can be found in Figure S9. Regardless, the *operando* XRD measurements were able to verify the *ex situ* data and the SEM/EDS investigations: inactive CAM plays a minor or no role.

Investigating binder stability via gas evolution

Gas evolution during electrochemical cycling has been reported to adversely affect the state of health of batteries. Although it is not as apparent as in liquid-electrolyte-based cells, gassing occurs for SSBs in the first few cycles. Overall, material degradation from the reaction of released gases with the electrode constituents appears to be less significant for the latter cells. Nevertheless, the sulfide solid electrolytes are degrading over time as a result of outgassing of the active material.

Together with the results from EIS, XRD, and SEM, we assume that differences in the chemical/electrochemical stability of the polymer binder in the system have a significant influence on the overall performance of the SSB cells. *Operando* gassing studies via DEMS were thus performed to determine the stability of the different binders based on the resulting gas evolution. To this end, NCM622 was cycled at a rate of C/20 and 45°C in the voltage range of 2.9–5.0 V versus Li⁺/Li. The higher charge cutoff voltage (5.0 versus 4.4 V) and temperature (45°C versus 25°C) were chosen with the intention of increasing the evolution of highly reactive singlet oxygen (¹O₂) from the CAM lattice and observing its potential influence on the components in the cathode sheets, especially the binder material. The respective cells were cycled for three cycles, and gas evolution was observed with decreasing amounts in

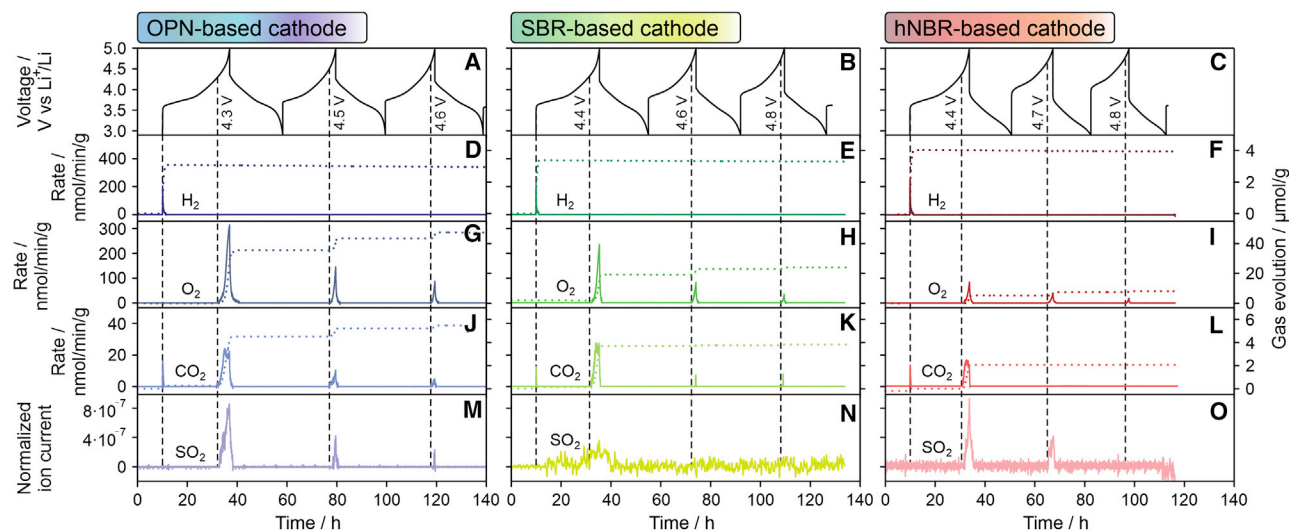


Figure 6. Gassing behavior of SSB cells using different polymer binders

(A–C) Voltage profiles and corresponding time-resolved evolution rates (left y axis) and cumulative amounts (right y axis) for (D–F) H₂, (G–I) O₂, and (J–L) CO₂, as well as the normalized ion currents for (M–O) SO₂. The SSB cells consisted of a slurry-cast cathode (uncoated NCM622, β-Li₃PS₄) with 2.0 wt % OPN, SBR, or hNBR binder and 1.0 wt % VGCF conductive additive, a Li₆PS₅Cl solid-electrolyte pellet separator, and an indium anode.

consecutive cycles at increasing onset voltages (from ~4.3 to 4.6/4.8 V) (Figures 6A–6C). Four gases were detected: H₂, O₂, CO₂, and SO₂. The evolution of H₂ ($m/z = 2$) only occurred at the beginning of the first charge cycle and could be attributed to the reduction of trace water at the anode (Figures 6D–6F).³³ For O₂ evolution, the cells are required to achieve >80% SOC.^{34,35} This condition was met for all cells, and the mass signal ($m/z = 32$) showed a sharp peak (Figures 6G–6I) with onset voltages of ~4.3 V for OPN-based cathodes and ~4.4 V for SBR- and hNBR-based cathodes in the initial cycle. The origin of O₂ evolution has been proposed in the literature to be a consequence of the destabilization of the layered Ni-rich oxide lattice at high voltages (>4.5 V versus Li⁺/Li).^{34,35} Although the OPN-based cell was able to reach ~89% SOC (243 mAh/g_{NCM622}), the SBR- and hNBR-based cells only achieved ~86% (235 mAh/g_{NCM622}) and ~80% (220 mAh/g_{NCM622}), respectively. The cumulative amount of O₂ evolved in the first cycle was ~36, 18, and 5 μmol/g_{NCM622} for OPN, SBR, and hNBR, respectively. This difference in O₂ evolution is due to the difference in SOC, because the amount follows an exponential-like relationship with SOC after reaching the 80% threshold. As seen in Figure S10, the SBR-based cathode followed a similar evolution progression to the OPN-based cathode, despite showing about 50% lower O₂ evolution.

The CO₂ mass signal ($m/z = 44$) for SSB cells predominantly stems from electrochemical decomposition of residual surface carbonates on the CAM particles, which is typically indicated by a sharp peak with an onset voltage > 4.2 V (Figures 6J–6L).^{36–38} However, a peak was also observed at the beginning of charging. In conventional liquid-electrolyte cells, CO₂ evolution at the start would be associated with an electrochemical reduction of the organic carbonate electrolyte. However, this is not applicable to SSBs. It could be postulated that the CO₂ evolution is correlated with side reactions at the anode, given that both H₂ evolution and CO₂ evolution occur almost simultaneously.³⁹ In general, we hypothesize that there are three possible sources for CO₂ evolution above 4.2 V: (1) electrochemical decomposition of residual surface carbonates, (2) chemical oxidation of the polymer binder, and (3) oxidation of the carbon additive. However, it has been shown in the literature that carbon additives are relatively stable

against the released oxygen from the NCM lattice⁴⁰ and therefore should not contribute to the observed CO₂ evolution. This leaves us with scenarios 1 and 2, which we elaborate upon when discussing about SO₂ evolution, because the two mass signals are believed to be correlated. Interestingly, when zooming into the gas evolution of both O₂ and CO₂ during the first cycle, we noticed a double peak for CO₂ for the OPN- and SBR-based cathodes (Figure S11). For the hNBR-based cathode, no distinct double peak was observed due to the lower SOC.

As is typical for SSB cells containing lithium thiophosphate solid electrolytes, a sharp peak corresponding to the mass signal $m/z = 64$ (SO₂) was detected (Figures 6M–6O). The mass signal of SO₂ is normalized with respect to the carrier-gas mass signal $m/z = 4$ (He) and represents at best a semiquantitative comparison. The formation of SO₂ could be attributed to the reaction between the solid electrolyte and the reactive oxygen released from the CAM at high voltages and from the electrochemical decomposition of residual surface carbonates.^{36–38,41} This is in agreement with the observed onset of SO₂ evolution, coinciding with both the O₂ and CO₂ signals. For hNBR-based cathodes, the SO₂ ion current exhibited an intensity similar to that of OPN-based cathodes, despite only showing ~14% of the O₂ evolution compared with the latter during the first cycle. The higher intensity of the SO₂ ion current in the hNBR-based cathode suggests that the solid electrolyte in these electrodes is less stable, supporting the arguments used in the discussion of the EIS data. The acrylonitrile groups of hNBR apparently exhibit ion-dipole interactions with the lithium ions of sulfide solid electrolytes, making it more vulnerable to side reactions. In contrast, SBR-based cathodes showed a more damped signal, indicating reduced SO₂ evolution, which cannot be simply explained by the lower amount of evolved O₂.

In an attempt to explain the damped SO₂ signal for the SBR-based cathodes, we hypothesize several possibilities: (1) coverage of the solid electrolyte and/or active material particles with polymer binder, preventing short-lived ¹O₂ from reaching the solid electrolyte; (2) reaction of evolved SO₂ with functional groups of the binder; and (3) preferential reaction of reactive oxygen with the binder instead of the solid electrolyte. For this discussion, a more in-depth analysis of the mass signal $m/z = 44$ was required. Specifically, both OPN- and SBR-based cathodes with a near identical SOC were needed for quantitative comparison, because CO₂ evolution, like O₂ evolution, shows an exponential-like relationship with the SOC (Figure S10). To this end, slurry-cast electrodes with LiNbO₃-coated NCM622 CAM were prepared and electrochemically tested. Representative first-cycle voltage profiles at a rate of C/10 and 25°C and the specific discharge capacities and Coulombic efficiencies over 20 cycles are shown in Figures 7A and 7B. Evidently, SSB cells with the LiNbO₃-coated NCM622 clearly outperformed those using uncoated CAM (Figure 5). This result was not unexpected and further indicates the effectiveness of the protective coating to mitigate decomposition reactions at the interfaces. OPN was capable of delivering the largest initial specific charge and discharge capacities of ~199 and 170 mAh/g_{NCM622} (~2 mAh/cm²), respectively (~85% versus ~77% Coulombic efficiency for uncoated NCM622). For SBR, lower specific capacities of ~192 and 164 mAh/g_{NCM622} were achieved (~85% versus ~75% Coulombic efficiency for uncoated NCM622). The protective surface coating was most beneficial for the hNBR-based cathode, improving both first-cycle specific discharge capacity and Coulombic efficiency by ~55% and 33%, respectively. Despite the similar initial irreversibility among the three polymer binders, the Coulombic efficiency of the hNBR-based cathode required four more cycles to stabilize above 99.5%, compared with two cycles for the OPN- and SBR-based cathodes. This suggests that more side reactions are occurring, especially in the initial cycles. However, an in-depth analysis would require

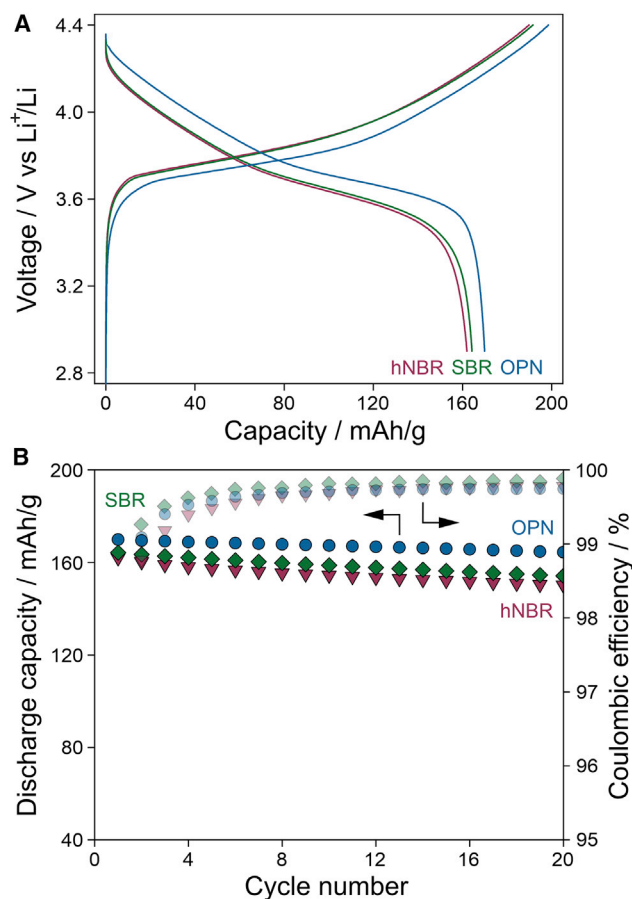


Figure 7. Cycling performance of SSB cells using different polymer binders

(A) First-cycle charge/discharge curves of slurry-cast cathodes (LiNbO_3 -coated NCM622, $\beta\text{-Li}_3\text{PS}_4$) with 2.0 wt % polymer binder (blue, OPN; green, SBR; pink, hNBR) and 1.0 wt % VGCF conductive additive. LTO and $\text{Li}_6\text{PS}_5\text{Cl}$ served as the pellet anode and solid-electrolyte separator, respectively, in the SSB cells.

(B) Specific discharge capacities (dark blue/green/pink) over 20 cycles and corresponding Coulombic efficiencies (light blue/green/pink).

further investigations. After 20 cycles, the specific discharge capacities decayed, as expected, corresponding to fade rates per cycle of $\sim 0.17\%$, 0.32% , and 0.39% for OPN, SBR, and hNBR, respectively. This result marks a significant improvement over the SSB cells using uncoated NCM622 CAM.

Such slurry-cast LiNbO_3 -coated NCM622 cathodes were then used in operando DEMS studies, and the gassing behavior of the corresponding SSB cells is shown in Figure 8 (for OPN and SBR) and Figure S12 (for hNBR). With a near-identical SOC for both OPN- and SBR-based cathodes (~ 250 versus 249 $\text{mAh/g}_{\text{NCM622}}$), we analyzed the evolution of O_2 , CO_2 , and SO_2 . The total amounts of O_2 detected after the first cycle were ~ 205 and 161 $\mu\text{mol/g}_{\text{NCM622}}$ for OPN and SBR, respectively, thus about an order of magnitude larger than what was observed for the uncoated NCM622 cathodes. The increased amounts help with the analysis of the gas evolution trends. The higher SOC also led to the appearance of an additional redox peak at ~ 4.6 V versus Li^+/Li (see differential capacity plots in Figure S13), which might be indicative of oxygen redox.^{34,42,43} In addition, we did not observe a damped signal for the SBR-based cathode with regard to the SO_2 . This was to be expected because the larger amount of

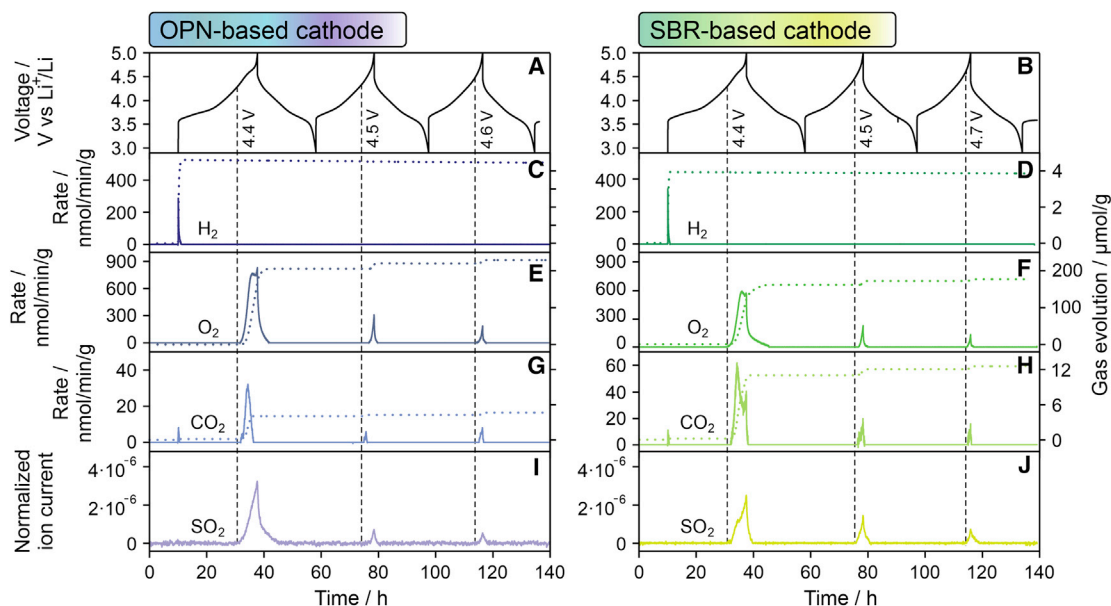


Figure 8. Gassing behavior of SSB cells using different polymer binders

(A and B) Voltage profiles and corresponding time-resolved evolution rates (left y axis) and cumulative amounts (right y axis) for (C and D) H₂, (E and F) O₂, and (G and H) CO₂, as well as the normalized ion currents for (I and J) SO₂. The SSB cells consisted of a slurry-cast cathode (LiNbO₃-coated NCM622, β-Li₃PS₄) with 2.0 wt % OPN or SBR binder and 1.0 wt % VGCF conductive additive, a Li₆PS₅Cl solid-electrolyte pellet separator, and an indium anode.

evolved O₂ would mean that there are plenty of reacting agents (¹O₂) available to both the polymer binder and the solid electrolyte. Nevertheless, the CO₂ evolution was more significant in the SBR-based cell. Because of the different gassing behavior of the uncoated and coated NCM622 cathodes, we are able to draw some conclusions here. We hypothesize that the first CO₂ peak (of the double peak at high voltages) is a result of the electrochemical decomposition of surface carbonates, whereas the second one results from possible reactions between the reactive oxygen and the binder material. Given that chemical oxidation of liquid electrolytes has been proposed in the literature,³⁴ it would be possible for ¹O₂ to attack the carbon chains/functional groups of the binder to produce CO₂.^{44,45} The double peak seen for CO₂ supports the hypothesis of a chemical oxidation of the binder. Moreover, the CO₂ evolution (second peak) was most pronounced in the SBR-based cathode. Reactive oxygen has been shown to be capable of reacting with polymers possessing an alkene chain (units),⁴⁴ and among the three materials, SBR is the only binder possessing one.

Finally, we try to explain the depressed SO₂ evolution seen for the SBR-based cathode using uncoated NCM622. We postulate that O₂ (probably ¹O₂) reacts with both the SBR binder and the solid electrolyte. To justify this, we bring some values into context. First, the LiNbO₃-coated NCM622 cathodes showed a (maximum) first-cycle normalized SO₂ ion current of 3.2×10^{-6} and 2.5×10^{-6} for OPN and SBR, respectively. The overall increase in ion current, compared with SSB cells using uncoated NCM622 (Figure 6), is due to the larger amounts of evolved O₂. As a result, the depressed SO₂ signal is not observed, because there is enough ¹O₂ to react with both the binder and the solid electrolyte. Second, despite showing less O₂ evolution, the SBR-based cathode exhibited 2–3 times more CO₂ evolution than the OPN-based electrode. Third, comparing the total amount of CO₂ evolution for both the uncoated and the LiNbO₃-coated NCM622 cathodes, we noticed that it remained similar for the OPN-based electrode at 4–5 μmol/g_{NCM622}, whereas that of the SBR-based electrode increased by a factor of about three (~11.0 versus 3.7 μmol/g_{NCM622}). The NCM622 particles used were all from the

same batch and therefore should have a similar amount of residual surface carbonates. Consequently, the additional CO₂ evolved from the SBR-based LiNbO₃-coated NCM622 cathode originated from a different source. In conclusion, these observations agree with our hypothesis that the alkene chain in SBR binder reacts with O₂ through a pathway that entails the formation of CO₂.

In conclusion, slurry-cast cathodes with electrochemical performance on par with powder-based, pelletized SSBs were produced with the help of DoE (Table S3). In addition, the optimization obtained for unprotected NCM622 CAM was transferable to LiNbO₃-coated NCM622, delivering high discharge capacities and showing good capacity retention and thus providing a methodology for the production of slurry-cast cathodes with different types of CAMs. Most importantly, the slurry-cast cathodes displayed similar cyclability but with increased reproducibility, which is necessary for use in future studies. When optimizing for electrochemical performance, slurry-cast cathodes with OPN binder and VGCF conductive additive were found to outperform other binder/carbon combinations. The type of binder and carbon additive and their respective content did affect the cycling performance to varying degrees. Not surprisingly, the well-performing electrode sheets all contained a low fraction of binder. JMP 14 extrapolated an optimum combination of 1.0 wt % OPN binder and 0.5 wt % VGCF conductive additive. However, slurry-cast cathodes with low binder content (<2.0 wt %) were susceptible to crack formation and delamination during cell preparation. For SSB sheet-based electrodes to be commercially viable, they have to be fabricated via continuous processing methods, in which they are usually subjected to strong mechanical forces during bending and shearing. Hence, in this study, the mechanical stability of the cathode sheet was also taken into consideration. The overall mechanical stability was found to largely depend on the binder content, with the other parameters, such as the type of binder and carbon additive, having a low degree of influence. A compromise between electrochemical performance and processability was achieved at 2.7 wt % OPN and 0.5 wt % VGCF. The measured cycling performance of SSB cells using a slurry-cast cathode with the optimal parameters corroborated the robustness of the model. Further understanding of the results from the DoE approach and the model built was provided by EIS, SEM/EDS, and XRD measurements. Lastly, operando gas analysis confirmed the (electro-)chemical stability of OPN. In addition, the correlation among O₂ evolution, CO₂ evolution, and SO₂ evolution allowed for hypotheses of reaction pathways, suggesting that polymer binders possessing alkene chains/units or functional groups that could potentially destabilize the solid electrolyte are unfavorable, especially at high voltages when in use with a layered Ni-rich oxide cathode material.

EXPERIMENTAL PROCEDURES

Resource availability

Lead contact

Further information and requests for resources should be directed to and will be fulfilled by the lead contact, Jun Hao Teo (jun.teo@kit.edu).

Materials availability

This study did not generate new reagents.

Data and code availability

The authors declare that the data supporting the findings are available within the article and the supporting information. All other data are available from the lead contact upon reasonable request.

Materials

Electrode sheets were prepared using pristine (unprotected) NCM622 (60% Ni, BASF)¹² powder as the CAM. The solid electrolytes, β -Li₃PS₄ (BASF) and argyrodite Li₆PS₅Cl (NEI), with room-temperature ionic conductivities of ~0.2 and 2 mS/cm, respectively, were applied as received. Three polymer binder materials were used for the study: OPN (Oppanol N 150 from BASF, average molecular weight [M_w] = 3.1×10^6 g/mol), hNBR (Therban LT 1707 VP from Arlanxeo, $M_w = 5.5 \times 10^5$ g/mol), and SBR (45 wt % styrene from Sigma Aldrich, $M_w \approx 6 \times 10^5$ g/mol).^{27,46,47} Super C65 carbon black (Timcal) and VGCF as electronically conductive additives were both dried at 300°C in a vacuum overnight before use. The LiNbO₃-coated NCM622 was prepared by coating a 1 wt % sol-gel-derived LiNbO₃ surface layer onto the pristine CAM.^{48–50} All materials were handled and stored in an argon glovebox from MBraun ([O₂] < 0.1 ppm, [H₂O] < 0.5 ppm).

DoE

The mass fractions of the two carbon additives, Super C65 and VGCF, were chosen to vary between 0.5 and 1.5 wt % (with a 0.5 wt % increment), whereas the content of the three polymer binders was chosen to vary between 1.0 and 3.0 wt % (with a 1.0 wt % increment). In other words, there were three variables with three levels and one variable with two levels. A classical, full factorial design of the cathode composite would thus require 54 ($3 \cdot 3 \cdot 3 \cdot 2$) experiments. Our customized experimental design reduced the number of required experiments to 23 (Table S1). The optimization was done with response variables quantifying the electrochemical and mechanical performance. Mechanical properties (processability) are represented by the results of two in-house mechanical tests, namely, bending and punching tests. To simplify the analysis, we assigned an arbitrary numerical scale to assess qualitative observations, so the higher number represents better processability. For the punching tests, round electrodes were punched from the cathode sheet with a circular geometry (9 mm diameter). They are rated according to the following scale: 4 = no mechanical deformation, 3 = edge delamination, 2 = delamination and cracking, and 1 = unprocessable (Figure S2). In case of the bending tests, the electrodes were tensioned at both ends and subjected to a rolling motion along a metal pipe (1 mm diameter) at varying bending angles. They are rated as follows: 4 = no mechanical deformation, 3 = delamination, 2 = delamination and cracking, and 1 = unprocessable. Several process-related parameters were fixed and excluded from the experimental design based on prior knowledge.

Cell assembly and electrochemical measurements

For the 23 DoE experimental runs, the SSB cells consisted of a slurry-cast cathode (9 mm diameter), a solid-electrolyte pellet separator (10 mm diameter), and a pellet anode (10 mm diameter). A specialized cell setup containing two stainless-steel dies and a plastic (polyether ether ketone, PEEK) ring was used. First, 65 mg of β -Li₃PS₄ was compressed at a pressure of ~125 MPa. The cathode was then punched into a circular geometry (2.0–2.4 mAh/cm² areal capacity), placed on top of the solid-electrolyte separator layer, and subsequently compressed at ~375 MPa. Lastly, 60 mg of anode composite was pressed onto the other side of the solid-electrolyte pellet at ~125 MPa. The anode composite was prepared by mixing 300 mg of carbon-coated LTO (NEI) with 100 mg of Super C65 carbon black and 600 mg of β -Li₃PS₄ at 140 rpm for 30 min in a 70 mL milling jar (Fritsch) with 10 zirconia balls (10 mm diameter) under an argon atmosphere using a planetary ball mill. For all subsequent electrochemical testing, SSB cells consisting of a slurry-cast cathode, a Li₆PS₅Cl pellet separator (100 mg), and a pellet anode (60 mg) were used. The anode composite was prepared in a fashion similar to that described earlier but with Li₆PS₅Cl as the solid electrolyte. During electrochemical testing, a stack pressure of ~80 MPa was maintained.

Galvanostatic charge/discharge measurements were performed at 25°C and at a rate of C/10 (1C = 180 mA/g_{N_{CM622}}) in the voltage range between 1.35 and 2.85 V versus Li₄Ti₅O₁₂/Li₇Ti₅O₁₂ (equal to ~2.9–4.4 V versus Li⁺/Li) using a Maccor battery cycler.

SUPPLEMENTAL INFORMATION

Supplemental information can be found online at <https://doi.org/10.1016/j.xcrp.2021.100465>.

ACKNOWLEDGMENTS

This study was supported by BASF SE. J.H.T. is grateful to the Federal Ministry of Education and Research (Bundesministerium für Bildung und Forschung, BMBF) for funding within the project ARTEMYS (03XP0114J). F.S. acknowledges financial support from Fonds der Chemischen Industrie (FCI) through a Liebig scholarship. The authors thank P. Hartmann (BASF SE), J. Kulisch (BASF SE), and X. Wu (BASF SE) for fruitful project discussions. Parts of this research were carried out at the light source PETRA III at DESY, a member of the Helmholtz Association (HGF). We thank M. Tolkiehn for assistance in using beamline P24 (EH2).

AUTHOR CONTRIBUTIONS

Conceptualization, J.H.T. and T.B.; methodology, J.H.T. and D.T.; software, D.T.; validation, J.H.T.; formal analysis, J.H.T., F.S., D.T., S.S., and Y.M.; investigation, J.H.T.; resources, M.B., J.J., and T.B.; writing – original draft, J.H.T. and T.B.; writing – review & editing, J.H.T., F.S., D.T., S.S., M.B., J.J., and T.B.; supervision, M.B., J.J., and T.B.; project administration, J.H.T. and T.B.; funding acquisition, J.J. and T.B.

DECLARATION OF INTERESTS

The authors declare no competing interests.

Received: February 18, 2021

Revised: April 14, 2021

Accepted: May 20, 2021

Published: June 15, 2021

REFERENCES

- Wang, Q., Ping, P., Zhao, X., Chu, G., Sun, J., and Chen, C. (2012). Thermal runaway caused fire and explosion of lithium ion battery. *J. Power Sources* 208, 210–224.
- Janek, J., and Zeier, W.G. (2016). A solid future for battery development. *Nat. Energy* 1, 16141.
- Kerman, K., Luntz, A., Viswanathan, V., Chiang, Y.-M., and Chen, Z. (2017). Review—practical challenges hindering the development of solid state Li ion batteries. *J. Electrochem. Soc.* 164, A1731–A1744.
- Sakuda, A., Hayashi, A., and Tatsumisago, M. (2013). Sulfide solid electrolyte with favorable mechanical property for all-solid-state lithium battery. *Sci. Rep.* 3, 2261.
- McGrogan, F.P., Swamy, T., Bishop, S.R., Eggleton, E., Porz, L., Chen, X., Chiang, Y.-M., and Van Vliet, K.J. (2017). Compliant yet brittle mechanical behavior of Li₂S-P₂S₅ lithium-ion-conducting solid electrolyte. *Adv. Energy Mater.* 7, 1602011.
- Richards, W.D., Miara, L.J., Wang, Y., Kim, J.C., and Ceder, G. (2016). Interface stability in solid-state batteries. *Chem. Mater.* 28, 266–273.
- Wolfenstine, J., Allen, J.L., Sakamoto, J., Siegel, D.J., and Choe, H. (2018). Mechanical behavior of Li-ion-conducting crystalline oxide-based solid electrolytes: a brief review. *Ionics* 24, 1271–1276.
- Wan, J., Xie, J., Kong, X., Liu, Z., Liu, K., Shi, F., Pei, A., Chen, H., Chen, W., Chen, J., et al. (2019). Ultrathin, flexible, solid polymer composite electrolyte enabled with aligned nanoporous host for lithium batteries. *Nat. Nanotechnol.* 14, 705–711.
- Zhou, J., Qian, T., Liu, J., Wang, M., Zhang, L., and Yan, C. (2019). High-safety all-solid-state lithium-metal battery with high-ionic-conductivity thermoresponsive solid polymer electrolyte. *Nano Lett.* 19, 3066–3073.
- Ito, S., Fujiki, S., Yamada, T., Aihara, Y., Park, Y., Kim, T.Y., Baek, S.-W., Lee, J.-M., Doo, S., and Machida, N. (2014). A rocking chair type all-solid-state lithium ion battery adopting Li₂O-ZrO₂ coated LiNi_{0.8}Co_{0.15}Al_{0.05}O₂ and a sulfide based electrolyte. *J. Power Sources* 248, 943–950.
- Aihara, Y., Ito, S., Omoda, R., Yamada, T., Fujiki, S., Watanabe, T., Park, Y., and Doo, S. (2016). The electrochemical characteristics and applicability of an amorphous sulfide-based solid ion conductor for the next-generation solid-state lithium secondary batteries. *Front. Energy Res.* 4, 18.
- Strauss, F., Bartsch, T., de Biasi, L., Kim, A.-Y., Janek, J., Hartmann, P., and Brezesinski, T. (2018). Impact of cathode material particle size on the capacity of bulk-type all-solid-state batteries. *ACS Energy Lett.* 3, 992–996.
- Doux, J.-M., Yang, Y., Tan, D.H.S., Nguyen, H., Wu, E.A., Wang, X., Banerjee, A., and Meng, Y.S. (2020). Pressure effects on sulfide electrolytes for all solid-state batteries. *J. Mater. Chem. A Mater. Energy Sustain.* 8, 5049–5055.
- Piper, D.M., Yersak, T.A., and Lee, S.-H. (2013). Effect of compressive stress on electrochemical

- performance of silicon anodes. *J. Electrochem. Soc.* **160**, A77–A81.
15. Fitzhugh, W., Ye, L., and Li, X. (2019). The Effects of Mechanical Constriction on the Operation of Sulfide Based Solid-State Batteries. *J. Mater. Chem. A Mater. Energy Sustain.* **7**, 23604–23627.
 16. Doux, J.-M., Nguyen, H., Tan, D.H.S., Banerjee, A., Wang, X., Wu, E.A., Jo, C., Yang, H., and Meng, Y.S. (2020). Stack pressure considerations for room-temperature all-solid-state lithium metal batteries. *Adv. Energy Mater.* **10**, 1903253.
 17. Wang, M.J., Choudhury, R., and Sakamoto, J. (2019). Characterizing the Li-solid-electrolyte interface dynamics as a function of stack pressure and current density. *Joule* **3**, 2165–2178.
 18. Fergus, J.W. (2010). Ceramic and polymeric solid electrolytes for lithium-ion batteries. *J. Power Sources* **195**, 4554–4569.
 19. Schnell, J., Günther, T., Knoche, T., Vieider, C., Köhler, L., Just, A., Keller, M., Passerini, S., and Reinhart, G. (2018). All-solid-state lithium-ion and lithium metal batteries—paving the way to large-scale production. *J. Power Sources* **382**, 160–175.
 20. Schnell, J., Knörzer, H., Imbsweiler, A.J., and Reinhart, G. (2020). Solid versus liquid—a bottom-up calculation model to analyze the manufacturing cost of future high-energy batteries. *Energy Technol. (Weinheim)* **8**, 1901237.
 21. Lee, K., Kim, S., Park, J., Park, S.H., Coskun, A., Jung, D.S., Cho, W., and Choi, J.W. (2017). Selection of binder and solvent for solution-processed all-solid-state battery. *J. Electrochem. Soc.* **164**, A2075–A2081.
 22. Yamamoto, M., Terauchi, Y., Sakuda, A., and Takahashi, M. (2018). Binder-free sheet-type all-solid-state batteries with enhanced rate capabilities and high energy densities. *Sci. Rep.* **8**, 1212.
 23. Rosero-Navarro, N.C., Kinoshita, T., Miura, A., Higuchi, M., and Tadanaga, K. (2017). Effect of the binder content on the electrochemical performance of composite cathode using $\text{Li}_6\text{PS}_5\text{Cl}$ precursor solution in an all-solid-state lithium battery. *Ionics* **23**, 1619–1624.
 24. Zhang, W., Leichtweiß, T., Culver, S.P., Koerver, R., Das, D., Weber, D.A., Zeier, W.G., and Janek, J. (2017). The detrimental effects of carbon additives in $\text{Li}_{10}\text{GeP}_2\text{S}_{12}$ -based solid-state batteries. *ACS Appl. Mater. Interfaces* **9**, 35888–35896.
 25. Koerver, R., Ayygün, I., Leichtweiß, T., Dietrich, C., Zhang, W., Binder, J.O., Hartmann, P., Zeier, W.G., and Janek, J. (2017). Capacity fade in solid-state batteries: interphase formation and chemomechanical processes in nickel-rich layered oxide cathodes and lithium thiophosphate solid electrolytes. *Chem. Mater.* **29**, 5574–5582.
 26. Walther, F., Randau, S., Schneider, Y., Sann, J., Rohnke, M., Richter, F.H., Zeier, W.G., and Janek, J. (2020). Influence of carbon additives on the decomposition pathways in cathodes of lithium thiophosphate-based all-solid-state batteries. *Chem. Mater.* **32**, 6123–6136.
 27. Ates, T., Keller, M., Kulisch, J., Adermann, T., and Passerini, S. (2019). Development of an all-solid-state lithium battery by slurry-coating procedures using a sulfidic electrolyte. *Energy Storage Mater.* **17**, 204–210.
 28. Strauss, F., Stepien, D., Maibach, J., Pfaffmann, L., Indris, S., Hartmann, P., and Brezesinski, T. (2020). Influence of electronically conductive additives on the cycling performance of argyrodite-based all-solid-state batteries. *RSC Advances* **10**, 1114–1119.
 29. Bielefeld, A., Weber, D.A., and Janek, J. (2020). Modeling effective ionic conductivity and binder influence in composite cathodes for all-solid-state batteries. *ACS Appl. Mater. Interfaces* **12**, 12821–12833.
 30. Koerver, R., Zhang, W., de Biasi, L., Schweidler, S., Kondrakov, A.O., Kolling, S., Brezesinski, T., Hartmann, P., Zeier, W.G., and Janek, J. (2018). Chemo-mechanical expansion of lithium electrode materials—on the route to mechanically optimized all-solid-state batteries. *Energy Environ. Sci.* **11**, 2142–2158.
 31. Bartsch, T., Kim, A.-Y., Strauss, F., de Biasi, L., Teo, J.H., Janek, J., Hartmann, P., and Brezesinski, T. (2019). Indirect state-of-charge determination of all-solid-state battery cells by X-ray diffraction. *Chem. Commun. (Camb.)* **55**, 11223–11226.
 32. Chen, K., Shinjo, S., Sakuda, A., Yamamoto, K., Uchiyama, T., Kuratani, K., Takeuchi, T., Orikasa, Y., Hayashi, A., Tatsumisago, M., et al. (2019). Morphological effect on reaction distribution influenced by binder materials in composite electrodes for sheet-type all-solid-state lithium-ion batteries with the sulfide-based solid electrolyte. *J. Phys. Chem. C* **123**, 3292–3298.
 33. Bernhard, R., Meini, S., and Gasteiger, H.A. (2014). On-line electrochemical mass spectrometry investigations on the gassing behavior of $\text{Li}_4\text{Ti}_5\text{O}_{12}$ electrodes and its origins. *J. Electrochem. Soc.* **161**, A497–A505.
 34. Jung, R., Metzger, M., Maglia, F., Stinner, C., and Gasteiger, H.A. (2017). Oxygen release and its effect on the cycling stability of $\text{LiNi}_x\text{Mn}_y\text{Co}_z\text{O}_2$ (NMC) cathode materials for Li-ion batteries. *J. Electrochem. Soc.* **164**, A1361–A1377.
 35. Jung, R., Strobl, P., Maglia, F., Stinner, C., and Gasteiger, H.A. (2018). Temperature dependence of oxygen release from $\text{LiNi}_0.8\text{Mn}_0.2\text{Co}_0.2\text{O}_2$ (NMC622) cathode materials for Li-ion batteries. *J. Electrochem. Soc.* **165**, A2869–A2879.
 36. Bartsch, T., Strauss, F., Hatsukade, T., Schiele, A., Kim, A.-Y., Hartmann, P., Janek, J., and Brezesinski, T. (2018). Gas evolution in all-solid-state battery cells. *ACS Energy Lett.* **3**, 2539–2543.
 37. Strauss, F., Teo, J.H., Schiele, A., Bartsch, T., Hatsukade, T., Hartmann, P., Janek, J., and Brezesinski, T. (2020). Gas evolution in lithium-ion batteries: solid versus liquid electrolyte. *ACS Appl. Mater. Interfaces* **12**, 20462–20468.
 38. Strauss, F., Teo, J.H., Maibach, J., Kim, A.-Y., Mazilkin, A., Janek, J., and Brezesinski, T. (2020). Li_2ZrO_3 -coated NCM622 for application in inorganic solid-state batteries: role of surface carbonates in the cycling performance. *ACS Appl. Mater. Interfaces* **12**, 57146–57154.
 39. Lux, S., Baldauf-Sommerbauer, G., and Siebenhofer, M. (2018). Hydrogenation of inorganic metal carbonates: a review on its potential for carbon dioxide utilization and emission reduction. *ChemSusChem* **11**, 3357–3375.
 40. Jung, R., Metzger, M., Maglia, F., Stinner, C., and Gasteiger, H.A. (2017). Chemical versus electrochemical electrolyte oxidation on NMC111, NMC622, NMC811, LNMO, and conductive carbon. *J. Phys. Chem. Lett.* **8**, 4820–4825.
 41. Mahne, N., Renfrew, S.E., McCloskey, B.D., and Freunberger, S.A. (2018). Electrochemical oxidation of lithium carbonate generates singlet oxygen. *Angew. Chem. Int. Ed. Engl.* **57**, 5529–5533.
 42. Sathiya, M., Rousse, G., Ramesha, K., Laisa, C.P., Vezin, H., Sougrati, M.T., Doublet, M.-L., Foix, D., Gonbeau, D., Walker, W., et al. (2013). Reversible anionic redox chemistry in high-capacity layered-oxide electrodes. *Nat. Mater.* **12**, 827–835.
 43. McCalla, E., Abakumov, A.M., Saubanère, M., Foix, D., Berg, E.J., Rousse, G., Doublet, M.-L., Gonbeau, D., Novák, P., Van Tendeloo, G., et al. (2015). Visualization of O-O peroxo-like dimers in high-capacity layered oxides for Li-ion batteries. *Science* **350**, 1516–1521.
 44. Clennan, E.L., and Pace, A. (2005). Advances in singlet oxygen chemistry. *Tetrahedron* **61**, 6665–6691.
 45. Ogilby, P.R. (2010). Singlet oxygen: there is indeed something new under the sun. *Chem. Soc. Rev.* **39**, 3181–3209.
 46. Riphaut, N., Strobl, P., Stiaszny, B., Zinkevich, T., Yavuz, M., Schnell, J., Indris, S., Gasteiger, H.A., and Sedlmaier, S.J. (2018). Slurry-based processing of solid electrolytes: a comparative binder study. *J. Electrochem. Soc.* **165**, A3993–A3999.
 47. Strauss, F., Teo, J.H., Janek, J., and Brezesinski, T. (2020). Investigations into the superionic glass phase of $\text{Li}_4\text{PS}_4\text{l}$ for improving the stability of high-loading all-solid-state batteries. *Inorg. Chem. Front.* **7**, 3953–3960.
 48. Takada, K., Ohta, N., Zhang, L., Fukuda, K., Sakaguchi, I., Ma, R., Osada, M., and Sasaki, T. (2008). Interfacial modification for high-power solid-state lithium batteries. *Solid State Ion.* **179**, 1333–1337.
 49. Ohta, N., Takada, K., Sakaguchi, I., Zhang, L., Ma, R., Fukuda, K., Osada, M., and Sasaki, T. (2007). LiNbO_3 -coated LiCoO_2 as cathode material for all solid-state lithium secondary batteries. *Electrochem. Commun.* **9**, 1486–1490.
 50. Kim, A.-Y., Strauss, F., Bartsch, T., Teo, J.H., Hatsukade, T., Mazilkin, A., Janek, J., Hartmann, P., and Brezesinski, T. (2019). Stabilizing effect of a hybrid surface coating on a Ni-rich NCM cathode material in all-solid-state batteries. *Chem. Mater.* **31**, 9664–9672.